

Influence Line-Based Design of Scissors-Type Bridge

Ichiro Ario ¹ , Yuta Hama ², Khongkham Chanthamanivong ³, Yuki Chikahiro ⁴ and Akimasa Fujiwara ¹ and Haicheng Ma ^{1,*} 

¹ Graduate School of Advanced Science and Engineering, Hiroshima University, Higashi-Hiroshima 739-8527, Japan

² Chodai Co., Ltd., Nishiku, Osaka City 550-0013, Japan

³ Luangnamtha Department of Public Works and Transport, Namtha 03000, Laos

⁴ Department of Water Environment and Civil Engineering, Shinshu University, Wakasato 4-17-1, Nagano 380-8553, Japan

* Correspondence: m224610@hiroshima-u.ac.jp

Abstract: Globally, large-scale natural disasters are occurring more frequently due to climatic and environmental changes. In addition, the disaster risk for infrastructures, mainly bridges, has become a vulnerability issue because reinforced concrete bridge structures are being directly exposed to the natural environment. Bridge structures linking cities or prefectures are destroyed in the aftermath of natural disasters and must be rebuilt. As a post-disaster measure, rapid reconstruction of damaged bridges and the reconnection of transportation systems between impacted locations and urban areas are the main problems encountered. This study aims to solve these problems through the application of a novel concept of an emergency bridge based on origami-inspired post-buckling theory, in conjunction with previous studies investigating the optimal deployable structure of scissors-type bridges. This study applied a novel design method for scissor-type bridges that use influence line diagrams and equilibrium equations. The proposed methods can determine the size of each member appropriately while providing the minimum and maximum values of the influence line border when carrying light vehicles by analyzing variations in the live load distribution on the structure. In the case of heavy vehicles passing over a bridge, the fundamental internal axial forces and bending moments were obtained, which provided design parameters for improving the load-carrying capacity of the structure. The proposed emergency bridge has a lower theoretical stress than that of a double-Warren truss.

Keywords: smart structure bridge; emergency bridge; coupling scissors-type bridge; scissors structure; deployable structure



Citation: Ario, I.; Hama, Y.; Chanthamanivong, K.; Chikahiro, Y.; Fujiwara, A.; Ma, H. Influence Line-Based Design of Scissors-Type Bridge. *Appl. Sci.* **2022**, *12*, 12170. <https://doi.org/10.3390/app122312170>

Academic Editor: José António Correia

Received: 22 October 2022

Accepted: 23 November 2022

Published: 28 November 2022

Publisher's Note: MDPI stays neutral with regard to jurisdictional claims in published maps and institutional affiliations.



Copyright: © 2022 by the authors. Licensee MDPI, Basel, Switzerland. This article is an open access article distributed under the terms and conditions of the Creative Commons Attribution (CC BY) license (<https://creativecommons.org/licenses/by/4.0/>).

1. Introduction

Natural disasters occur frequently. However, their impact is worsening and is becoming a challenging issue affecting global development.

Global warming has been noted as a factor in the increasing frequency of natural disasters, owing to development-related activities, such as industrial manufacturing, transportation, energy supply, and deforestation. Kumamoto (2020) and Hiroshima (2018) in Japan witnessed flooding and overflow of rivers, which led to the destruction of bridges (refer to Ario et al. (2021) [1,2]) and severed the mode of transportation between the two regions, as shown in Figure 1. The impact and probable reasons for demolition were investigated by Ario (2006) [3].

Previously, there were many kinds of temporary bridges in Japan that used different construction methods, such as the pre-girder bridge, kiln-dried truss, HS truss, Hi-BRIDGE construction, Hi-RoRo construction, double-Warren truss (hereinafter DWT) [4], and dry support bridge methods; these techniques for Accelerated Bridge Construction require between one and ten weeks for bridge assembly WFEL (2012) [5], Unibridge (2015) [6] (see

Figure 2a). The Army Forces Bridge required approximately 8 h and 80 soldiers for assembly (see Figure 2b). Bridge assemblies require extensive labor as well as high-capacity cranes.



Figure 1. Collapsed bridges due to flooding in Kumamoto, Japan (July 2020).



Figure 2. Types of temporary bridges and a military bridge in Japan. (a) A temporary bridge built by a company. (b) A temporary bridge built by the military.

Historically, the first emergency bridge, the Bailey Bridge, was proposed in 1943 by D. Bailey and was a modularized truss bridge. Studies have been conducted to evaluate the usability of lightweight materials such as fiber-reinforced plastic (FRP) (R. Wight (2006) [7]). Generally, the scissors-type structure (hereinafter SCI) uses FRP for domes and roofs (Perez (1965) [8], Zeigler (1976) [9], Escrig (1985) [10]), as shown in Figure 3b,c [11]. Harris (1975) [12] proposed a space structure for bridge construction. The deployable structures have demonstrated more complexity, such as the matrix formulation of macro-elements (Kwan & Pellegrino (1994) [13]), smart deployable skeletal structures for safety engineering (Pawłowski & Graczykowski et al. (2013) [14]), and a rapidly deployable bridge system (Thomas (2013) [15]).

In this paper, we propose the influence line method for a smart bridge engineering that employs the SCI to expand and fold itself within an hour with the requirement of only a few people (see Figure 3). This makes it possible to evacuate people from the bridge within a short time. Many types of mobile bridges (hereinafter MB), structures with expanding and folding equipment, have been patented previously by Ario (2006) [3]. A prototype deployable bridge based on origami principles was also developed by Ario & Nakazawa et al. (2013) [16]. Studies were conducted on the theory and design of a full-scale SCI (Chikahiro & Ario et al. (2016) [17]) and bridge design for scissors-type bridges based on Origami engineering (Hama & Ario et al. (2017) [18]). This study investigated the influence line (hereinafter I.L.) of axial forces, bending moments, and shear forces on the scissors structure to establish a practical design theory. The I.L. of the SCI was compared with the standard DWT model and advanced couple scissors-type bridge (hereinafter CSCI) models [19]. The concept involves moving live loads along the structure using a truck model.

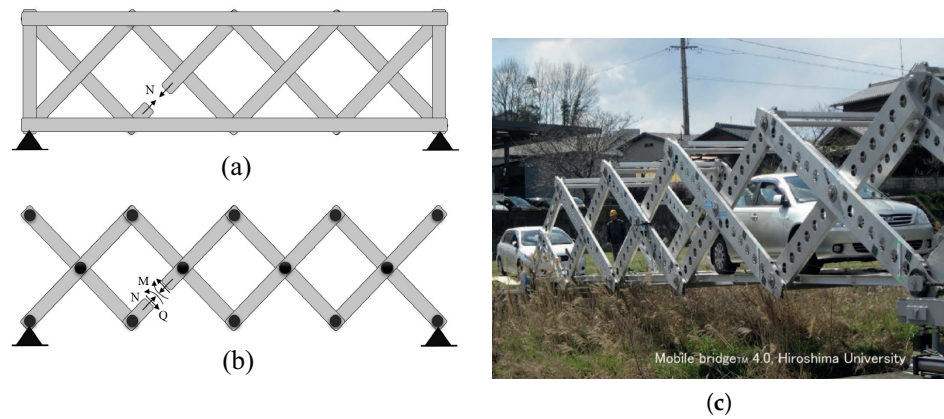


Figure 3. Types of emergency bridges. (a) Double Warren truss (DWT). (b) The scissors-type bridge (SCI). (c) The smart bridge [20].

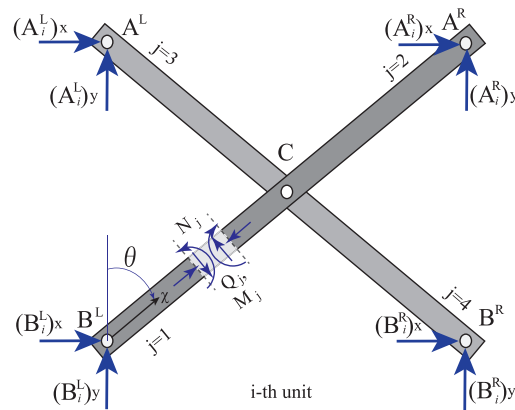


Figure 4. Definition of the coordinate system and sectional forces in a scissors unit structure.

2. The Equilibrium Theory

2.1. The Mechanism of the Scissors Structure Using the Cantilever Model

The two-unit scissors model depends on its boundary condition and the position of the applied load to each nodal point (see Figure 4). This model is based on a cantilever that consists of a pinned support point on the left-hand side B_1^L and A_1^L and P at point B_2^R . The rotation point of the scissor is denoted by C_1 , its length by λ , and its height by η [11] and/or [17] (see Figure 5).

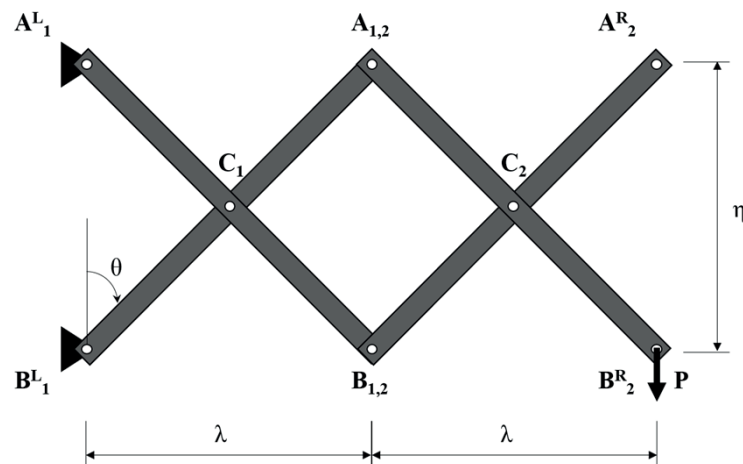


Figure 5. Two-units scissors structure by cantilever model.

In the equation, the external forces are on the left-hand side and internal forces (This implies that the force at the nodal point is $(\bullet^*)_\Phi$. $(\bullet^*)_\Phi \equiv [\bullet^* | A^L, B^L, C, A^R, B^R; * = \{L, R\}; \Phi = \{x, y\}]$, \bullet^* denotes nodal label.) are on the connection points $B_{1,2}$ and $A_{1,2}$ on the right-hand side. We obtain the following condition:

$$\begin{Bmatrix} (B_{1,2})_x \\ (B_{1,2})_y \\ (A_{1,2})_x \\ (A_{1,2})_y \end{Bmatrix} = \begin{Bmatrix} (B_1^R)_x \\ (B_1^R)_y \\ (A_1^R)_x \\ (A_1^R)_y \end{Bmatrix} + \begin{Bmatrix} (B_2^L)_x \\ (B_2^L)_y \\ (A_2^L)_x \\ (A_2^L)_y \end{Bmatrix} \tag{1}$$

Therefore, the relevant equilibrium equations are as follows:

$$\begin{Bmatrix} (B_{1,2}) \\ (A_{1,2}) \end{Bmatrix} = \begin{Bmatrix} (B_1^R) \\ (A_1^R) \end{Bmatrix} + \begin{Bmatrix} (B_2^L) \\ (A_2^L) \end{Bmatrix} \tag{2}$$

$$[L] \begin{Bmatrix} (B_1^L) \\ (A_1^L) \end{Bmatrix} = -[R] \begin{Bmatrix} (B_1^R) \\ (A_1^R) \end{Bmatrix} - \begin{Bmatrix} (C_1) \\ \mathbf{0} \end{Bmatrix} \tag{3}$$

$$[L] \begin{Bmatrix} (B_2^L) \\ (A_2^L) \end{Bmatrix} = -[R] \begin{Bmatrix} (B_2^R) \\ (A_2^R) \end{Bmatrix} - \begin{Bmatrix} (C_2) \\ \mathbf{0} \end{Bmatrix} \tag{4}$$

Here,

$$[L] = \left[\begin{array}{cc|cc} 1 & 0 & 1 & 0 \\ 0 & 1 & 0 & 1 \\ \hline -\eta & \lambda & 0 & 0 \\ 0 & 0 & \eta & \lambda \end{array} \right], \quad [R] = \left[\begin{array}{cc|cc} 1 & 0 & 1 & 0 \\ 0 & 1 & 0 & 1 \\ \hline 0 & 0 & \eta & -\lambda \\ -\eta & -\lambda & 0 & 0 \end{array} \right]$$

At each nodal point, a solution is obtained by applying the equation for each nodal point in the following order. Then, we obtain their forces in matrix form based on the following equation [17] and/or [20].

$$\begin{Bmatrix} (B_1) \\ (A_1) \end{Bmatrix} = -([L]^{-1}[R])^2 \begin{Bmatrix} (B_2) \\ (A_2) \end{Bmatrix} - [L]^{-1}[R] \begin{Bmatrix} (B_{1,2}) \\ (A_{1,2}) \end{Bmatrix} - [L]^{-1}[R][L]^{-1} \begin{Bmatrix} (C_2) \\ \mathbf{0} \end{Bmatrix} - [L]^{-1} \begin{Bmatrix} (C_1) \\ \mathbf{0} \end{Bmatrix} \tag{5}$$

In this solution, the right-hand side is subject to P at point $(B_2^R)_y = -P$ and the other nodal forces ($= 0$) in Equation (5), the unknown reaction forces for the two-unit SCI can be expressed as $(A_1^L)_x = -(B_1^L)_x = -P \tan \theta$ and $(A_1^L)_y = P, (B_1^L)_y = 0$.

A comparison of the theoretical predictions for the one and two-unit SCI shows that the vertical reaction forces are identical in both; however, the horizontal reaction forces are double of those in the vertical direction. Therefore, the horizontal reaction forces may become very high if the number of scissors units is increased [21].

2.2. The Mechanism of Scissors Structure Using Simple Support Model

A two-unit SCI model with nodal forces acting only on the hinge, pivot, and pin was supported at both ends, as shown in Figure 6. All members have the same length and angle of inclination θ , measured in the vertical direction. The length and height of the scissor unit are defined as λ and η . The left-hand scissors unit consists of nodes B_1^L, B_1^R, C_1, A_1^L and A_1^R , and the second scissors unit consists of nodes B_2^L, B_2^R, C_2, A_2^L and A_2^R . All nodal points are considered to be hinges. Loading is applied at nodal locations only; hence no bending moments were transmitted or applied at these nodal junctions [20,21].

The horizontal $(\bullet^*)_x$ and vertical $(\bullet^*)_y$ equilibrium equations for the left-hand side unit are as follows:

$$\begin{aligned}
 [R] \begin{Bmatrix} (B_1^R)_x \\ (B_1^R)_y \\ (A_1^R)_x \\ (A_1^R)_y \end{Bmatrix} &= -[L_1] \begin{Bmatrix} (B_1^L)_x \\ (B_1^L)_y \\ (B_2^R)_x \\ (B_2^R)_y \end{Bmatrix} - \begin{Bmatrix} (C_1)_x + (A_1^L)_x \\ (C_1)_y + (A_1^L)_y \\ \mathbf{0} \\ \eta(A_1^L)_x + \lambda(A_1^L)_y \end{Bmatrix} \\
 \begin{Bmatrix} (B_1^R)_x \\ (B_1^R)_y \\ (A_1^R)_x \\ (A_1^R)_y \end{Bmatrix} &= -[R]^{-1}[L_1] \begin{Bmatrix} (B_1^L)_x \\ (B_1^L)_y \\ (B_2^R)_x \\ (B_2^R)_y \end{Bmatrix} - [R]^{-1} \begin{Bmatrix} (C_1)_x + (A_1^L)_x \\ (C_1)_y + (A_1^L)_y \\ \mathbf{0} \\ \eta(A_1^L)_x + \lambda(A_1^L)_y \end{Bmatrix} \quad (6)
 \end{aligned}$$

Here,

$$[R] = \left[\begin{array}{cc|cc} 1 & 0 & 1 & 0 \\ 0 & 1 & 0 & 1 \\ \hline 0 & 0 & \eta & -\lambda \\ -\eta & -\lambda & 0 & 0 \end{array} \right], \quad [L_1] = \left[\begin{array}{cc|cc} 1 & 0 & 0 & 0 \\ 0 & 1 & 0 & 0 \\ \hline -\eta & \lambda & 0 & 0 \\ 0 & 0 & 0 & 0 \end{array} \right]$$

From the right-hand SCI, we obtain the equation as below.

$$\begin{aligned}
 [L] \begin{Bmatrix} (B_2^L)_x \\ (B_2^L)_y \\ (A_2^L)_x \\ (A_2^L)_y \end{Bmatrix} &= -[R_2] \begin{Bmatrix} (B_1^L)_x \\ (B_1^L)_y \\ (B_2^R)_x \\ (B_2^R)_y \end{Bmatrix} - \begin{Bmatrix} (C_2)_x + (A_2^R)_x \\ (C_2)_y + (A_2^R)_y \\ \eta(A_2^R)_x - \lambda(A_2^R)_y \\ \mathbf{0} \end{Bmatrix} \\
 \begin{Bmatrix} (B_2^L)_x \\ (B_2^L)_y \\ (A_2^L)_x \\ (A_2^L)_y \end{Bmatrix} &= -[L]^{-1}[R_2] \begin{Bmatrix} (B_1^L)_x \\ (B_1^L)_y \\ (B_2^R)_x \\ (B_2^R)_y \end{Bmatrix} - [L]^{-1} \begin{Bmatrix} (C_2)_x + (A_2^R)_x \\ (C_2)_y + (A_2^R)_y \\ \eta(A_2^R)_x - \lambda(A_2^R)_y \\ \mathbf{0} \end{Bmatrix} \quad (7)
 \end{aligned}$$

Here,

$$[L] = \left[\begin{array}{cc|cc} 1 & 0 & 1 & 0 \\ 0 & 1 & 0 & 1 \\ \hline -\eta & \lambda & 0 & 0 \\ 0 & 0 & \eta & \lambda \end{array} \right], \quad [R_2] = \left[\begin{array}{cc|cc} 0 & 0 & 1 & 0 \\ 0 & 0 & 0 & 1 \\ \hline 0 & 0 & 0 & 0 \\ 0 & 0 & -\eta & -\lambda \end{array} \right]$$

At nodes $(B_{1,2})$ and $(A_{1,2})$, the external forces $(B_{1,2})_y, (B_{1,2})_x, (A_{1,2})_y, (A_{1,2})_x$ are in equilibrium with the internal forces $(B_1^R)_y, (B_1^R)_x, (A_1^R)_y, (A_1^R)_x$ and $(B_2^L)_y, (B_2^L)_x, (A_2^L)_y, (A_2^L)_x$ (see Figure 6). The sum of the forces for each unit can be expressed as follows:

$$\begin{Bmatrix} (B_1^R)_x \\ (B_1^R)_y \\ (A_1^R)_x \\ (A_1^R)_y \end{Bmatrix} + \begin{Bmatrix} (B_2^L)_x \\ (B_2^L)_y \\ (A_2^L)_x \\ (A_2^L)_y \end{Bmatrix} = \begin{Bmatrix} (B_{1,2})_x \\ (B_{1,2})_y \\ (A_{1,2})_x \\ (A_{1,2})_y \end{Bmatrix} \quad (8)$$

Substitution Equation (6) and (7) into Equation (8) and rearranging will be as below:

$$\begin{aligned}
 [S] \begin{Bmatrix} (B_1^L)_x \\ (B_1^L)_y \\ (B_2^R)_x \\ (B_2^R)_y \end{Bmatrix} &= \begin{Bmatrix} (B_{1,2})_x \\ (B_{1,2})_y \\ (A_{1,2})_x \\ (A_{1,2})_y \end{Bmatrix} + [R]^{-1} \begin{Bmatrix} (C_1)_x + (A_1^L)_x \\ (C_1)_y + (A_1^L)_y \\ \mathbf{0} \\ \eta(A_1^L)_x + \lambda(A_1^L)_y \end{Bmatrix} \\
 &\quad + [L]^{-1} \begin{Bmatrix} (C_2)_x + (A_2^R)_x \\ (C_2)_y + (A_2^R)_y \\ \eta(A_2^R)_x - \lambda(A_2^R)_y \\ \mathbf{0} \end{Bmatrix} \quad (9)
 \end{aligned}$$

$$[S] = -[R]^{-1}[L_1] - [L]^{-1}[R_2] \quad (10)$$

If the determinant of $[S]$, which is the coefficient matrix corresponding to the vector $\{(B_1^L)_x, (B_1^L)_y, (B_2^R)_x, (B_2^R)_y\}^T$, is not 0, the reaction forces at the supports have a unique solution. Moreover, if the external forces are known, then Equation (10) can be solved by [21].

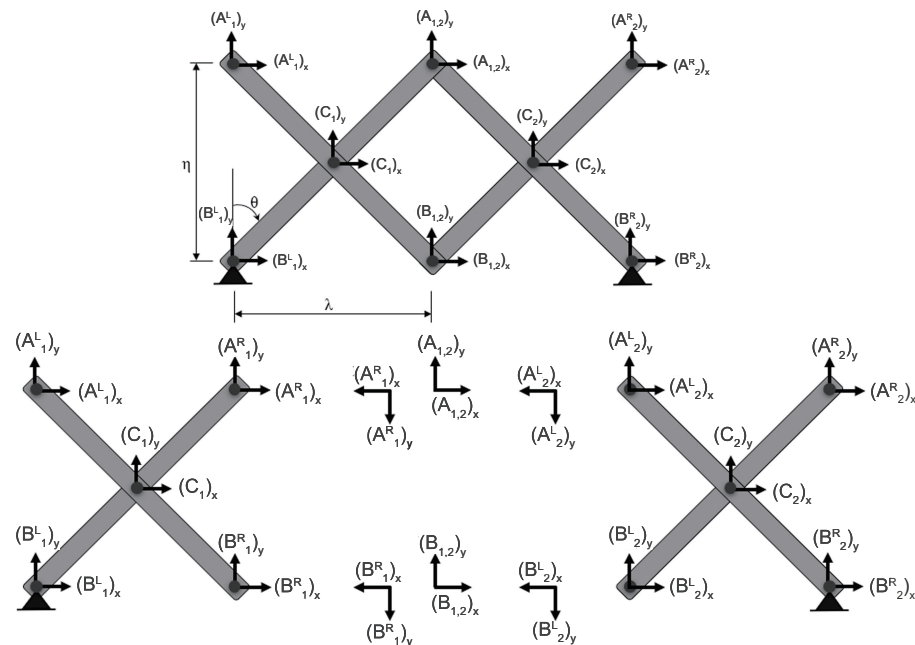


Figure 6. Two-units scissors structure by simple support model.

3. Scissors Bridge Design Method

In this section, we explain the calculation method of the I.L. for the scissors member using the calculation process described in the previous section. There are no existing studies on the design of a bridge with a scissor mechanism; therefore, a design method based on the I.L. for the structure has not yet been established. We attempted to generalize the I.L. of the scissors member by assuming an underfloor slab constructed using the theory of equilibrium dynamics of the scissors bridge [20,21], such that it can be generically designed for arbitrary case parameters.

3.1. Comparison with the Influence Line (I.L.) of a Truss

We confirmed the similarities of the I.L. of the diagonal member of the Warren Truss structure, which is the most general truss structure and the I.L. of the member of the scissors structure. The I.L. of Warren truss structure is generalized, and it is possible to design live loads by the bridge designer. For example, the axial force of the member of interest can be obtained using the straight line of the gradient of $1/\sin\theta$ for the axial force of the diagonal. However, the I.L. has not been formulated for the scissors structure. Considering the entire structure as one large beam and considering the vertical shearing force (Q), in the case of Warren Truss, the diagonal member resists the shearing force. However, in the case of the scissors structure, the scissors member resists the shearing force. We compared the I.L.s of the shear force (Q) of both structures and aimed at grasping and formulating the behavior of the I.L. of the scissors structure. The I.L.s of both the structures are shown in Figure 7. Considering the members at the same position, the comparison showed that the phases were reversed, but an I.L. with the same tendency was obtained using the 0–1 gradient straight line. Therefore, although the method of solving the section force of the scissors bridge differs significantly, as a bridge, the characteristics are the same as those of existing bridges. Therefore, it is possible to design a bridge against moving loads.

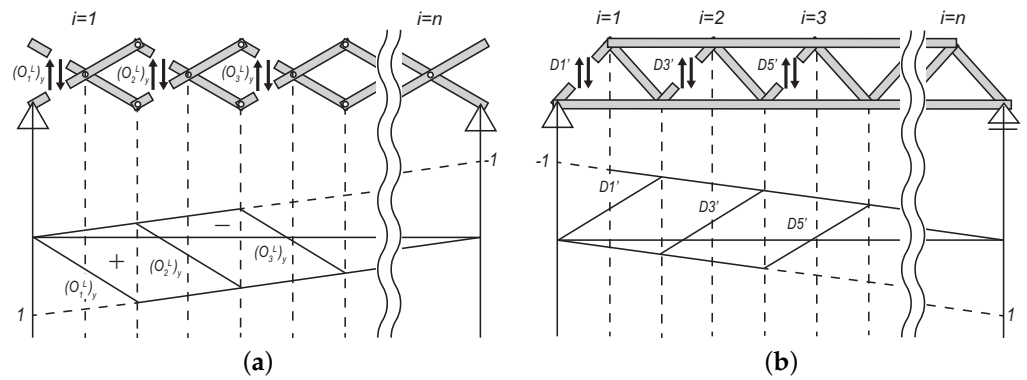


Figure 7. Comparison of examples of the I.L. (a) Sharing force for the scissors bridge. (b) Sharing force for a Warren truss bridge.

3.2. Design Method Using Influence Line (I.L.)

The I.L. is convenient for carrying out live loads design. The greatest advantage is that it is possible to easily obtain changes in the values of sectional force and displacement attributable to the moving loads using the longitudinal distance and area. To determine the I.L. of the section force and displacement of the scissors structure, the ordinate was first calculated by applying the unit load $P = 1$ to the line, assuming the slab (upper, middle, and lower roads). Further calculations are made by moving the load at interval length λ and repeating the same calculation. The scissors structure shows different distribution of sectional force for odd and even numbers. Therefore, between odd numbers with $2n + 1$ category ($n \geq 1$), it is maximised, as shown below. General equation of the I.L. of the members of the central unit, where the section force is the maximum in the scissors model for each case number, as shown below. For odd units ($2n + 1$), the I.L. of N_{n+1}^1 is expressed as follows:

$$\zeta = \begin{cases} \{\cos \theta + (n + 1) \sin \theta \tan \theta\} \zeta & , \zeta \in [0, \frac{n}{2n+1}] \\ -n\{(2 \cos \theta + \sin \theta \tan \theta)\zeta - \cos \theta - \sin \theta \tan \theta\} & , \zeta \in [\frac{n}{2n+1}, \frac{n+1}{2n+1}] \\ (\cos \theta - n \sin \theta \tan \theta)(\zeta - 1) & , \zeta \in [\frac{n+1}{2n+1}, 1] \end{cases}$$

Here, ζ is the ordinate, n is the number of units, θ is the deployment angle, L_s is the span length, and x denotes the distance from the left support point in the direction of the bridge axis. χ is the distance of the coordinate transformation in the member of axis direction. The parameter ξ is the normalized coordinate distance as $x/L_s \in [0, 1]$.

The I.L. of N_{n+1}^3 is expressed as

$$\zeta = \begin{cases} -(n + 1) \sin \theta \tan \theta \cdot \zeta & , \zeta \in [0, \frac{n}{2n+1}] \\ n \sin \theta \tan \theta (\zeta - 1) & , \zeta \in [\frac{n}{2n+1}, 1] \end{cases} \tag{11}$$

The I.L. of shearing force Q_{n+1}^1 expresses the following:

$$\zeta = \begin{cases} -n \sin \theta \cdot \zeta & , \zeta \in [0, \frac{n+1}{2n+1}] \\ (n + 1) \sin \theta (\zeta - 1) & , \zeta \in [\frac{n+1}{2n+1}, 1] \end{cases} \tag{12}$$

The I.L. of M_{n+1}^1 expresses the following:

$$\zeta = \begin{cases} -n\chi \sin \theta \cdot \zeta & , \zeta \in [0, \frac{n+1}{2n+1}] \\ (n + 1)\chi \sin \theta (\zeta - 1) & , \zeta \in [\frac{n+1}{2n+1}, 1] \end{cases} \tag{13}$$

For even units ($2n$), the I.L. of N_n^2 expresses the following:

$$\zeta = \begin{cases} -n \sin \theta \tan \theta \cdot \zeta & , \zeta \in \left[0, \frac{1}{2}\right] \\ n \sin \theta \tan \theta (\zeta - 1) & , \zeta \in \left[\frac{1}{2}, 1\right] \end{cases} \tag{14}$$

The I.L. of N_n^4 is expressed as

$$\zeta = \begin{cases} -(\cos \theta - n \sin \theta \tan \theta) \cdot \zeta & , \zeta \in \left[0, \frac{n-1}{2n}\right] \\ \{(2n - 1) \cos \theta + n \sin \theta \tan \theta\} \zeta - (n - 1) \cos \theta & , \zeta \in \left[\frac{n-1}{2n}, \frac{1}{2}\right] \\ (\cos \theta + n \sin \theta \tan \theta)(1 - \zeta) & , \zeta \in \left[\frac{1}{2}, 1\right] \end{cases}$$

The I.L. of shearing force Q_n^2 is expressed as follows:

$$\zeta = \begin{cases} n \sin \theta \cdot \zeta & , \zeta \in \left[0, \frac{1}{2}\right] \\ -n \sin \theta (\zeta - 1) & , \zeta \in \left[\frac{1}{2}, 1\right] \end{cases} \tag{15}$$

The I.L. of shearing force Q_n^4 is expressed as

$$\zeta = \begin{cases} (n + 1) \sin \theta \cdot \zeta & , \zeta \in \left[0, \frac{n-1}{2n}\right] \\ -(n - 1) \sin \theta (\zeta - 1) & , \zeta \in \left[\frac{n-1}{2n}, 1\right] \end{cases} \tag{16}$$

The I.L. of M_n^2 expresses the following:

$$\zeta = \begin{cases} n\chi \sin \theta \cdot \zeta & , \zeta \in \left[0, \frac{1}{2}\right] \\ -n\chi \sin \theta (\zeta - 1) & , \zeta \in \left[\frac{1}{2}, 1\right] \end{cases} \tag{17}$$

The I.L. of M_n^4 expresses the following:

$$\zeta = \begin{cases} (n + 1)\chi \sin \theta \cdot \zeta & , \zeta \in \left[0, \frac{n-1}{2n}\right] \\ -(n - 1)\chi \sin \theta (\zeta - 1) & , \zeta \in \left[\frac{n-1}{2n}, 1\right] \end{cases} \tag{18}$$

Based on these general equations, we could design the active load of main structural members of the scissors bridge, assuming a lower road slab with a single support state of fixed span length, number of units, and deployment angle.

4. The Influence Line of Scissors and Double-Warren Truss Structures

4.1. I.L. of DWT Structure

For DWT structure, only axial forces occurred at every nodal point of the structure, as shown in Figure 8. For each nodal point at the four corners and the central point of each unit, we obtain Equations (19) and (20). We can perform I.L. determination during unit load $(F_i)_y = -1$ subject to every single nodal point and it can be determined at the truss structure. The I.L. diagrams of every single node are obtained by moving the unit load along the distance by λ and calculating for another single nodal point (Hama & Ario et al. (2017) [18]).

$$\begin{bmatrix} 1 & \cos \theta & 0 \\ 0 & \sin \theta & 1 \end{bmatrix} \begin{Bmatrix} N_i^v \\ N_i^d \\ N_i^h \end{Bmatrix} = - \begin{Bmatrix} \pm (F_i)_y \\ (F_i)_x \end{Bmatrix} \tag{19}$$

$$\begin{bmatrix} \cos \theta & -\sin \theta \\ \cos \theta & \sin \theta \\ 0 & -1 \\ 0 & 1 \end{bmatrix}^T \begin{Bmatrix} N_{i-1}^d \\ N_i^d \\ N_{i-1}^h \\ N_i^h \end{Bmatrix} = - \begin{Bmatrix} \pm (F_i)_y \\ (F_i)_x \end{Bmatrix} \tag{20}$$

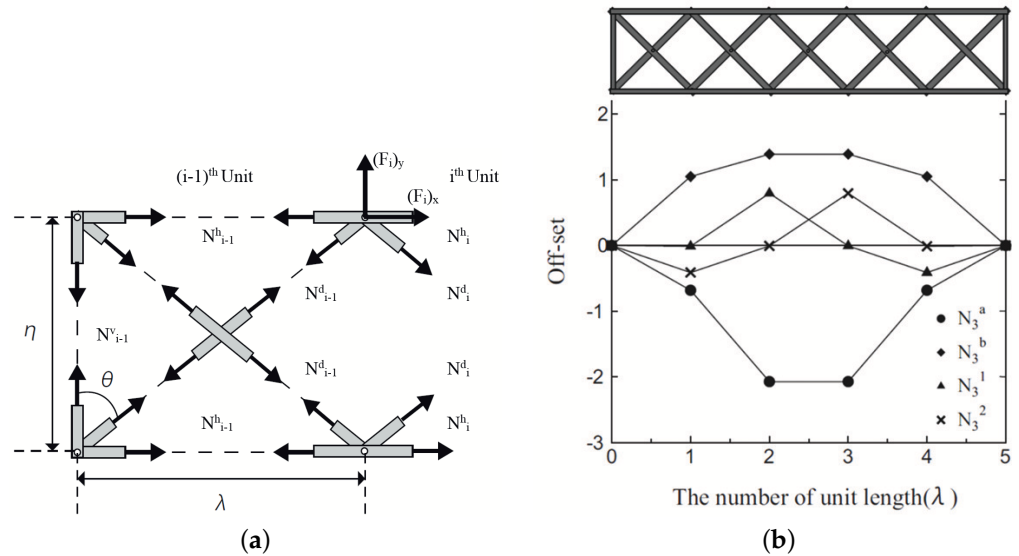


Figure 8. The sectional nodal forces and I.L. of axial force at 3rd unit of DWT. (a) The sectional nodal forces. (b) I.L. of axial force at 3rd unit of DWT.

4.2. I.L. of CSCI Structure

The CSCI is a combination of many scissors in one set that generates energy through homogeneous behavior. However, in the method of analysis in this paper, the I.L. of a deck is considered, and its load is subject to the main scissors structure in an orderly manner.

The I.L. analysis of CSCI is performed by the calculation of its section force members, and equilibrium equations of all nodal forces are obtained from Equations (21) and (22) by Hama and Ario et al. (2017) [18].

$$[L]b_i^L + [R]b_i^R + b_i^C = 0 \tag{21}$$

$$b_i^R + b_{i+1}^L = P_i \tag{22}$$

Here,

$$[L] = \begin{bmatrix} 1 & 0 & 1 & 0 \\ 0 & 1 & 0 & 1 \\ -\eta & \lambda & 0 & 0 \\ 0 & 0 & \eta & \lambda \end{bmatrix}, \quad [R] = \begin{bmatrix} 1 & 0 & 1 & 0 \\ 0 & 1 & 0 & 1 \\ 0 & 0 & \eta & -\lambda \\ -\eta & -\lambda & 0 & 0 \end{bmatrix}$$

$$b_i^* = \{(B_i^*)_x, (B_i^*)_y, (A_i^*)_x, (A_i^*)_y\}^T, \quad * = \{L \text{ or } R\}$$

$$b_i^C = \{(C_i)_x, (C_i)_y, 0, 0\}^T$$

$$P_i = \{(P_i^B)_x, (P_i^B)_y, (P_i^A)_x, (P_i^A)_y\}^T$$

The equations are obtained from the equilibrium condition of each nodal force in the horizontal and vertical axes, as well as the bending moment of the central point (pivot point C) by considering every member of the scissors unit. Therefore, the axial forces, shear

forces, and bending moment are calculated by their coordinates reversed to the member direction and using the following equations.

$$N_i^j = \pm(O_i^*)_x \sin \theta \pm (O_i^*)_y \cos \theta \quad (23)$$

$$Q_i^j = \pm(O_i^*)_x \cos \theta \pm (O_i^*)_y \sin \theta \quad (24)$$

$$M_i^j = \{\pm(O_i^*)_x \cos \theta \pm (O_i^*)_y \sin \theta\} \chi \quad (25)$$

where in the distance coordinate $0 \leq \chi \leq L_e/2$ from each corner node.

Then, the letters represent the following: N , axial force; Q , shear force; M , bending moment; O , point A or B points.

In the case of a four-unit SCI, the load $P = 1$ is subjected to every single nodal point substitution from point $B_{1,2} \sim B_{3,4}$. From a simple SCI, we obtained the I.L. of the axial forces, bending moments, and shear forces (see Figure 9).

In Figure 9a, the small SCI (black scissors structure) will be a deck of the bridge, and it is calculated using a two-unit simple SCI model, which is subject to a one-unit SCI (light gray SCI). Through structural analysis, we obtain the reaction forces from the 2-units SCI and its reaction forces are subjected to the main SCI from points $B_1^L \sim B_4^R$. The CSCI is analyzed by assuming load $\bar{P} = 1$ subject to the main SCI from points $B_{1,2} \sim B_{3,4}$ (see Figure 10a,b). Subsequently, we can obtain the I.L. of N , Q , and M using the load distribution by one unit and P -load, as shown in Figure 11a–c.

Furthermore, truck model H-25 in ASSHTO passes in two directions (from the left to the right side and from the right to the left side), at the highest loading point of this structure, the front wheel load of H-25 $P = 22.236$ kN and rear-wheel load $P = 88.946$ kN. From this, we obtained graphs of the axial forces, shear forces, and bending moments (see Figure 12a–c). Then, the small SCI will be analyzed with simple equations and reaction forces are obtained, which are subjected to every nodal point of the main structure. With the above, we consider the analysis of the five types of structural models in Figure 13.

4.3. Results and Discussions

The structural models shown in Figure 13 are designed using high strength low alloy steel, and the main hollow member has $400 \times 70 \times 15$ mm (height \times width \times thickness) and is 6000 mm in length. Hence, the model had a unit length of 4000 mm and a total length of approximately 16,000 mm. The Young's modulus is 200 GPa, shear modulus is 128.7 GPa, and density is 7.85 g/cm³. The yield strength was 275.8 MPa, whereas the tensile strength was 448 MPa.

The boundary condition was determined using simple pinned supports on both ends of the structure. The truck model H-25 was simulated using Autodesk Inventor, which provides the rear wheel ($18,140$ kgf $\times 0.5 = 9070$ kgf or 88.946 kN) subject to the highest bending moment point of a single structure (at nodal point $B_{2,3}$), and the front wheel will be subjected to nodal point $B_{1,2}$. Furthermore, the truck also reverses the front wheel at nodal point $B_{3,4}$ while the rear wheel is in the same position.

The simulation results in Table 1 show that the von Mises stress (VMS) for the Double Warren Truss structure (DWT) in Figure 14 was less than that of Coupling scissors-type structure (CSCI) Model A in Figure 15 by approximately 10%, while its displacement (hereinafter Disp.) and the structural weights remain lower for the two. Conversely, the VMS of CSCI Model B in Figure 15 is lower than DWT by approximately 2%, while its displacement and the structural weights are higher. The VMS of CSCI Model C in Figure 15 were lower than DWT by approximately 2%, while its structural weight is higher, and displacement is lower. The VMS of CSCI Model D in Figure 15 is lower than DWT by approximately 20%, while its structural weight is higher, and displacement is lower. The 1st principal stress (1st PS) and 3rd principal stress (3rd PS) are listed in Table 1.

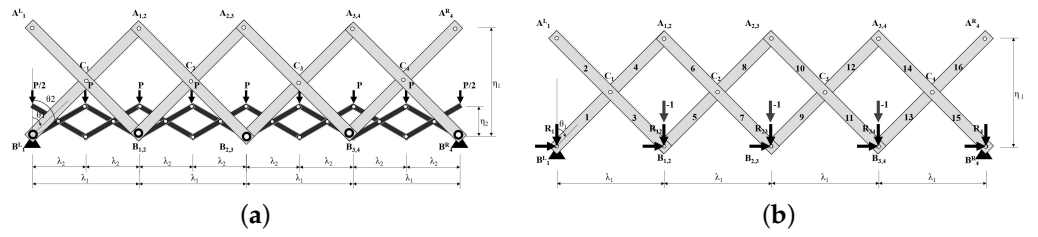


Figure 9. Assumptions of unit load $P = 1$ distributed to the coupling of a scissors-type structure. (a) The unit load $P = 1$ acting on the CSCI. (b) The unit load transferring to the main SCI.

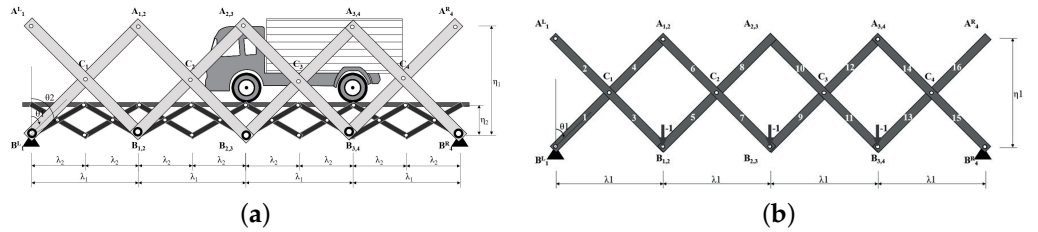


Figure 10. The load $P = 1$ distributes to the CSCI and the truck loading on the CSCI. (a) The truck loading on the CSCI. (b) The unit load transferring to the main SCI.

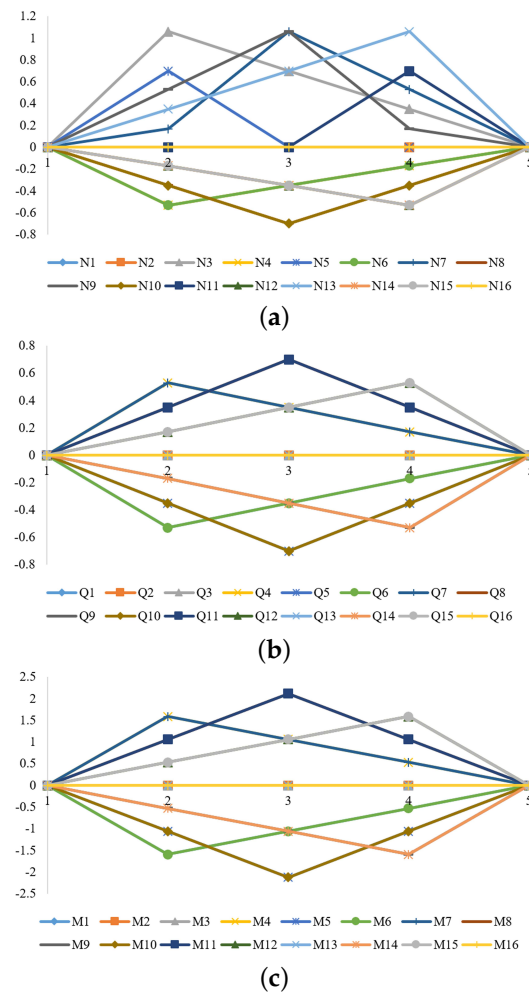


Figure 11. I.L. diagram of AFD, SFD, and BMD subject to the normal SCI structure by $P = 1$ loading. (a) I.L. of AFD N , $P = 1$ acting on the SCI. (b) I.L. of SFD Q , $P = 1$ acting on the SCI. (c) I.L. of BMD M , $P = 1$ acting on the SCI.

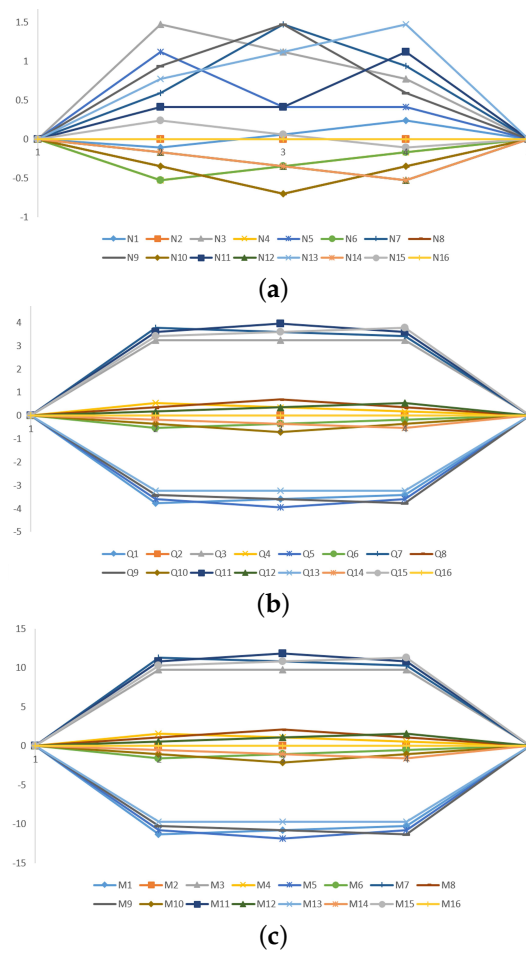


Figure 12. I.L. diagram of AFD N , SFD Q , and BMD M of CSCI by H-25 truck. (a) I.L. of AFD N at the normal CSCI. (b) I.L. of SFD Q at the middle of CSCI. (c) I.L. of BMD M at the middle of CSCI.

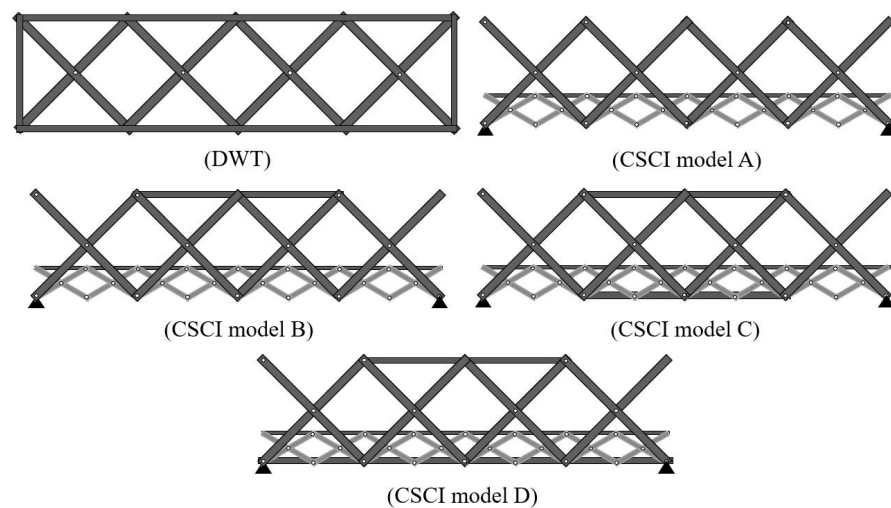


Figure 13. The types of structural models.

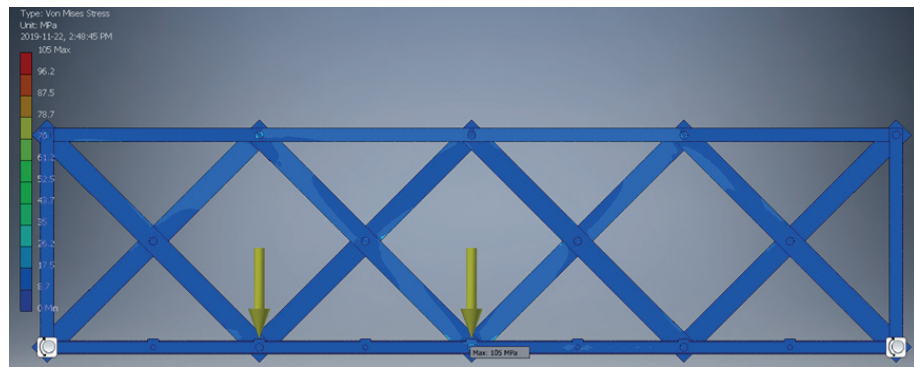
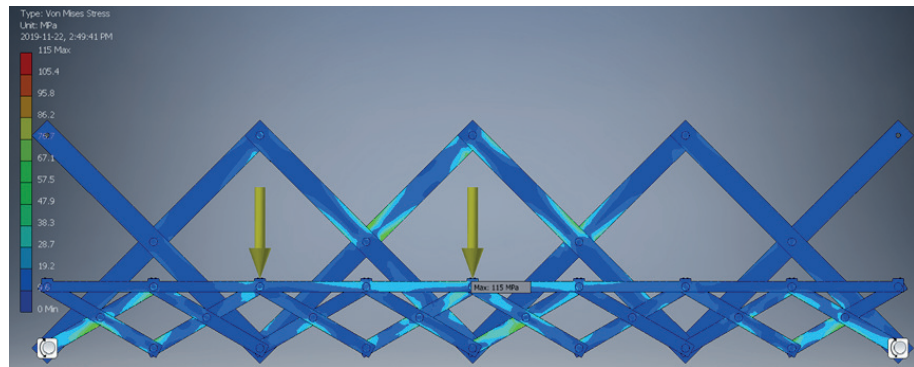
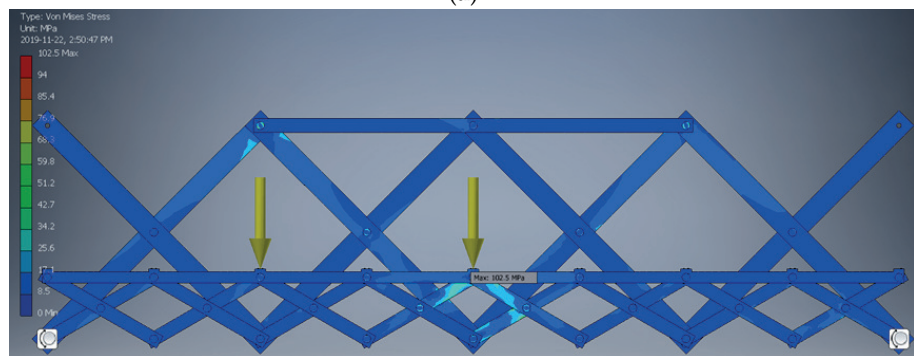


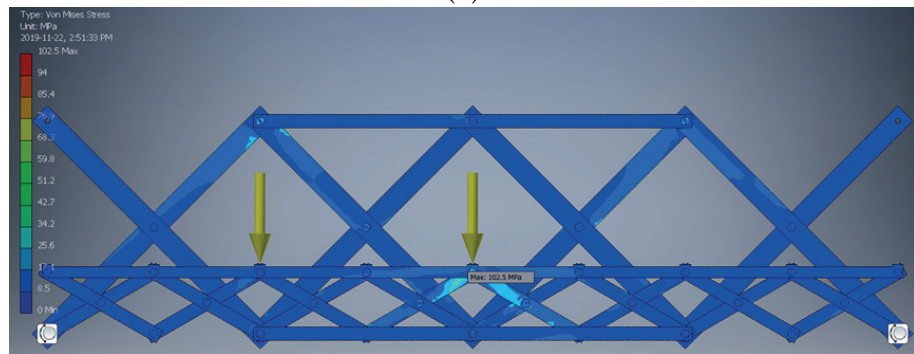
Figure 14. The simulation result of DWT model



(a)

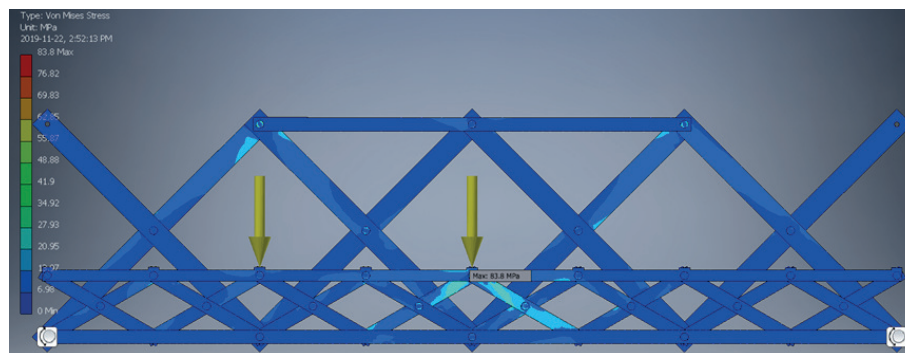


(b)



(c)

Figure 15. Cont.



(d)

Figure 15. The simulation results of CSCI models. (a) CSCI model-A. (b) CSCI model-B. (c) CSCI model-C. (d) CSCI model-D.

Table 1. The simulation results of DWT & CSCI models A, B, C, D by Autodesk Inventor 2018.

Model Names	Mass kgf	Disp. mm	VMS MPa	1st PS MPa	3rd PS MPa	Mass Ratio	Disp. Ratio	VMS Ratio
DWT	999.15	7.52	104.96	103.13	12.61	1.00	1.00	1.00
CSCI (A)	1027.46	9.15	114.98	114.01	25.67	1.03 (1.00)	1.22 (1.00)	1.10 (1.00)
CSCI (B)	1111.48	8.22	102.49	104.81	32.47	1.11 (1.08)	1.09 (0.89)	0.98 (0.89)
CSCI (C)	1195.5	6.53	102.49	105.45	28.80	1.20 (1.16)	0.86 (0.71)	0.98 (0.89)
CSCI (D)	1277.83	5.75	83.79	85.63	25.72	1.28 (1.24)	0.76 (0.63)	0.80 (0.73)

5. Conclusions

This study investigated the I.L. diagrams of axial forces, bending moments, and shear forces on the structure of DWT and CSCI models. The concept involves moving live loads along the structure using truck model H-25 (22,675 kgf). The maximum axial force, shear force, and bending moment were obtained. To summarize, we can conclude the following:

1. Using the equilibrium mechanics theory of the SCI, we obtained the equations of the primary I.L.s of the sectional forces of the frame elements with pin-connections. Furthermore, their I.L. has been used to design the maximum loading point of a structure by the equilibrium equations and the assumed loading from the small SCI to the main SCI.
2. The authors numerically analyzed the CSCI structure, resulting in a normal SCI structure that is used currently.
3. The I.L. at which the axial force N is higher than $P = 1$ unit at 2nd, 3rd, 4th nodal points, is 1.1 unit (+10%); Shear force Q is lower than $P = 1$ unit at 3rd nodal point, the I.L. is 0.7 unit (−30%); Bending moment M is higher than $P = 1$ unit at 3rd nodal point, the I.L. is 2.2 unit (+120%).
4. A comparison between the stress of DWT and CSCI structure showed that the stress of CSCI (A) is greater than DWT by 10%, while the stress of CSCI (B) is lower than DWT by 2%, but displacement is only over 10%. Moreover, in the case where the comparative model is CSCI (A), we can observe that the CSCI (B) clearly shows potential that when upper reinforcement member is applied, the stress reduces by 11%, while the mass increases by only 8%.

The results in this paper showed that if we develop CSCI (B) as an emergency bridge, it will be more significant than other models because of its deployment mechanism and efficiency. However, it is still difficult to deploy CSCI (D). CSCI (D) can be used for other applications in coupling scissor-type devices in the future.

Author Contributions: Conceptualization, I.A. and Y.C.; methodology, Y.H. and I.A.; software, Y.H. and K.C.; validation, Y.C. and I.A., formal analysis, Y.H. and K.C.; investigation, Y.H. and K.C.; resources, Y.H. and I.A.; data curation, Y.C.; writing—original draft preparation, Y.H. and K.C.; writing—review and editing, K.C. and H.M.; visualization, K.C. and Y.H.; supervision, I.A.; funding acquisition, A.F. All authors have read and agreed to the published version of the manuscript.

Funding: This research was funded by Japan Society for the Promotion of Science grant number 19H00784.

Institutional Review Board Statement: Not applicable.

Informed Consent Statement: Not applicable.

Data Availability Statement: Some or all data, models, or code that support the findings of this study are available from the corresponding author upon reasonable request. All data, models, and code generated or used during the study appear in the submitted article.

Conflicts of Interest: The authors declare no conflict of interest.

References

1. Ario, I.; Yamashita, T.; Tsubaki, R.; Kawamura, S.; Uchida, T.; Watanabe, G.; Fujiwara, A. Investigation of Bridge Collapse Phenomena due to Heavy Rain Floods: Structural, Hydraulic, and Hydrological Analysis. *J. Bridge Eng.* **2022**, *27*, 04022073. [CrossRef]
2. Ario, I.; Watanabe, G.; Shibata, T.; Kaita, T.; Kawamura, S. Investigation Report Damage Survey of Bridge Collapse Phenomena in Misasa River Due to Torrential Rain in Western Japan Flood in 2018. Academic Research Repository in Hiroshima University. 2022; pp. 1–35. Available online: <https://ir.lib.hiroshima-u.ac.jp/files/public/5/52397/20220607153724188335/0606a-Hiroshima-broken-bridges2018-2g.pdf> (accessed on 10 August 2022).
3. Ario, I. Structure with the Expanding and Folding Equipment in Hiroshima University. Japan Patent No. 2006-037668, 15 February 2006.
4. Production Information of KD Bridge Wtruss. Available online: <http://www.hirose-net.com/pdf/catalog/07.pdf> (accessed on 10 August 2022).
5. WFEL Ltd. Dry Support Bridge. Available online: <https://www.wfel.com/project/dry-support-bridge> (accessed on 10 August 2022).
6. Unibridge Company. Emergency Bridges of Unibridge. Available online: <http://www.unibridge.net.au/solution/emergency-bridges/> (accessed on 10 August 2022).
7. Wight, R.; Erki, M.; Shyu, C.; Tanovic, R.; Heffernan, P. Development of FRP Short-Span Deployable Bridge—Experimental Results. *J. Bridge Eng.* **2006**, *11*, 489–498. :4(489). [CrossRef]
8. Perez, P.E. Three Dimensional Reticular Structure. U.S. Patent NO. 3185164, 25 May 1965. Available online: <https://patents.google.com/patent/US3185164A/en> (accessed on 10 August 2022)..
9. Zeigler, T.R. Collapsible Self-Supporting Structure. U.S. Patent No. 3968808, 13 July 1976. Available online: <https://patents.google.com/patent/US3968808A/en> (accessed on 10 August 2022).
10. Escrig, F. Expandable space structure. *Int. J. Space Struct.* **1985**, *1*, 79–91. [CrossRef]
11. Ario, I.; Chikahiro, Y. A new type of bridge mobilebridge registered to super-quickly recover a bridge. *World J. Eng. Technol.* **2015**, *3*, 170. [CrossRef]
12. Harris, M.F. Stress Balanced Extendible Boom Structure. U.S. Patent No. 3877544, 15 April 1975.
13. Kwan, A.; Pellegrino, S. Matrix formulation of macro-elements for deployable structures. *Comput. Struct.* **1994**, *50*, 237–254. [CrossRef]
14. Pawłowski, P.; Graczykowski, C.; Holnicki-Szulc, J.; Ario, I. Smart, deployable skeletal structures for safety engineering. In Proceedings of the 6th ECCOMAS Thematic Conference on Smart Structures and Materials, Torino, Italy, 24–26 June 2013; pp. 1–10.
15. Thomas, G.R.; Sia, B.J. A rapidly deployable bridge system. In Proceedings of the Structures Congress (ASCE), Pittsburgh, PA, USA, 2–4 May 2013; pp. 656–667.
16. Ario, I.; Nakazawa, M.; Tanaka, Y.; Tanikura, I.; Ono, S. Development of a prototype deployable bridge based on origami skill. *Autom. Constr.* **2013**, *32*, 104–111. [CrossRef]
17. Chikahiro, Y.; Ario, I.; Nakazawa, M. Theory and design study of a full-scale scissors-type bridge. *J. Bridge Eng.* **2016**, *21*, 9. [CrossRef]
18. Hama, Y.; Ario, I.; Chikahiro, Y.; Adachi, K.; Watson, A. Origami inspired deployable & movable bridge for disaster relief. In *Foot-bridge 2017 Berlin-Tell A Story*, 6–8.9; Technische Universität Berlin: Berlin, Germany, 2017. [CrossRef]
19. Chanthamanivong, K.; Ario, I.; Chikahiro, Y. Smart design of coupling scissors-type bridge. *Structures* **2021**, *30*, 206–216. [CrossRef]

20. Ario, I.; Chikahiro, Y.; Tanikura, I.; Ono, S.; Nakazawa, M.; Nakatani, S.; Yamada, K.; Nakamura, S.; Tanaka, Y.; Tsubaki, R. Consider recovering method by mobile bridge how to install a disaster. In Proceedings of the of the 7th Special Symposium for Reducing Disaster, Kumamoto, Japan, December 2016. (In Japanese)
21. Chikahiro, Y.; Ario, I.; Nakazawa, M.; Ono, S.; Holnicki-Szulc, J.; Pawlowski, P.; Graczykowski, C.; Watson, A., Experimental and numerical study of full-scale scissor type bridge. *Autom. Constr.* **2016**, *71*, 171–180. [[CrossRef](#)]